EXPERIMENT NO. 1

HOT-WIRE ANEMOMETRY:
FLOW IN THE WAKE OF A CIRCULAR CYLINDER

Submitted by:

Kush Jani

AEROSPACE AND OCEAN ENGINEERING DEPARTMENT

VIRGINIA POLYTECHNIC INSTITUTE AND STATE UNIVERSITY

BLACKSBURG, VIRGINIA

27 SEPTEMBER 2025

EXPERIMENT PERFORMED 15 SEPTEMBER 2025

LAB TEACHING ASSISTANT: NAGA NITISH CHAMALA

I. Abstract

This report contains an investigation into the use of hot-wire anemometry enabled through Virginia Tech's AOE Undergraduate Teaching Laboratory. The primary objective of this investigation was the comparison of mean velocity and turbulence intensity curves from flow undergoing both laminar and turbulent boundary layer separation. In order to meet this goal, a Constant Temperature Anemometer (CTA) system that controlled a hot-film anemometer was calibrated against a pitot-static pressure probe yielding coefficients for the King's Law governing equation which were validated in their veracity by means of first-order linear polynomial fit made on linearized values of acquired data. Results from this investigation validate the fundamental aerodynamic principle behind drag-based design through induced turbulent separation as the collected data definitively showed the creation of a smaller deficit in mean velocity inside the wake for the induced turbulent boundary layer separation case than the natural laminar boundary layer separation case. Time-history data collected further showed the characteristic properties of critical points in the wake of a disturbance in the flow, namely regarding the greater turbulence intensity that is present in the shear layer found at the edges of the wake than the centerline of the wake. Lastly, the investigation demonstrated the unique capabilities of hot-wire anemometry as a means for aerodynamic analysis in turbulent flow regimes, such as those found in wakes, through the greater sampling rate achieved by hot-wire anemometry as a result of its electrically based mechanism.

INVESTIGATION OF FLUID FLOW IN THE WAKE OF A CYLINDER VIA HOT WIRE ANEMOMETRY

Kush Jani[1]
Virginia Tech, Blacksburg, VA 24060

II. Introduction

The goals of this study are:

1. To calibrate a hot-film anemometer probe using known flow velocities and establish its response characteristics according to King's Law.
2. To utilize the calibrated probe to measure the mean velocity and turbulence profiles in the wake of a circular cylinder.
3. To compare the wake characteristics resulting from both laminar and turbulent boundary layer separation on the cylinder.
4. To analyze the unsteady velocity fluctuations at distinct locations within the flow field.

These goals were accomplished by utilizing Virginia Tech's 0.7m Subsonic Open-Jet Wind Tunnel due to its capabilities in generating a uniform flow along with the aerodynamic testing equipment necessary for gleaning properties of said flow. The wind tunnel utilized is showcased in Fig. 1, and the aerodynamic testing equipment is also displayed in Fig. 2. The theoretical basis for this experiment is summarized as follows:

Hot-wire anemometry is a technique in aerodynamic testing utilized for measuring fluid velocity through the convective heat transfer caused by air flow over a heated element such as a wire. For this lab experiment, a Constant Temperature Anemometer (CTA) system was used which allows a feedback control loop to adjust the electrical current through the wire to maintain a constant temperature and thus constant resistance. The additional voltage used by the system as a result of maintaining this constant temperature is thus a direct relationship between the heat transfer which itself is dependent on fluid velocity and allows for calculations to be done to derive flow velocity from the measurable voltage change. The relationship between flow and voltage is given by King's Law

$$E^2 = A + Bu^n \tag{1}$$

where E is the anemometer bridge voltage, u is the fluid velocity, and A, B, and n are calibration constants. For this experiment, the value of n was assumed to be 0.45 due to constraints on time to perform the experiment as $n = 0.45$ is a common value for hot-wire probes. The calibration constants A and B were found through the course of the investigation as described in the calibration techniques section.

One of the primary advantages of hot-wire anemometry is a by-product of the use of electrical signals for derivation of the fluid flow velocity as this enables the measurements to be rapid and thus capable of measuring fluid flow velocity even for unsteady turbulent flow which has chaotic fluctuations in velocity. This can be shown formally through the mean velocity which $\bar{u}$ defined through equation

$$\bar{u} = \lim_{T\to\infty} \frac{1}{T} \int_0^T u(t)dt \tag{2}$$

where $u(t)$ is the instantaneous velocity and T is time. The variance of the signal output by the testing equipment can be calculated as the root-mean-square (RMS) of the velocity fluctuations σ which is the square root of the variance given as

$$\sigma^2 = \overline{(u - \bar{u})^2} \tag{3}$$

where u is the aforementioned instantaneous velocity and $\bar{u}$ is the mean velocity. This experiment applies these foundational concepts to the investigation of wake behind a circular cylinder during both laminar and turbulent flow to characterize the state of the boundary layer prior to separation dominated flow downstream in the wake.

[1] Undergraduate student, Aerospace & Ocean Engineering Department.

The remainder of this report is as follows: Section III describes the experimental setup, equipment, and techniques used to perform the experiment alongside an aside into the MATLAB code utilized to generate calibration values for constants A and B required by King's Law as discussed briefly for Eq. 1. Section IV describes the results from the experiment regarding the identification of characteristics in the wake of the cylinder as the flow begins to separate while also describing areas of improvement for further experimentation. Finally, Section V contains the discussion for the experiment and the insights garnered from the methodology employed as well as a brief discussion of the uncertainties which are tabulated in Appendix A.

III. Apparatus and Techniques

A. Open Jet Wind Tunnel

The experiment was conducted in the Virginia Tech 0.7m Subsonic Open-Jet Wind Tunnel where a cylinder 5.5 inches in diameter was mounted in the test section. A trip strip was also installed on the cylinder during the turbulent testing in order to induce a turbulent flow with boundary layer separation since the wind tunnel is not natively capable of achieving flows in turbulent regimes. The wind tunnel is a blower type open circuit facility that consists of aluminum composite panels installed on an aluminum frame with a steel base. The blower is a 30hp BC-SW Size 365 Twin City centrifugal fan discharging to a 4 meter long diffuser of 6° followed by a settling chamber of dimensions 1.47 by 1.78 m which contains honeycomb cells of 0.01m by 0.09m long as well as three fiberglass turbulence reduction screens of a 55% open area ratio via 0.3mm-diameter gaps. This is then followed by a 5.5:1 contraction nozzle prior to discharging into the open test-section and subsequent jet catcher, which contains two fiberglass high-loss screens located 1.2 m past the nozzle exit to minimize flow entering the lab, as shown in Fig. 1. The fan is capable of a maximum RPM of 1180, which corresponds to a maximum freestream velocity in the test-section of approximately 30 m/s, and is controlled by the Open-Jet Wind Tunnel Operation Control MATLAB code. Data acquisition was done through the LabVIEW software which recorded the output voltage from the CTA system as shown in Fig. 3 alongside the aforementioned MATLAB wind tunnel operation code which recorded atmospheric conditions of the lab.

B. Hot-Film Probe and Constant Temperature Anemometer System

The hot-wire probe utilized in the experiment was a Thermo-Systems Inc. (TSI) type 1212-20 hot-film probe which is made up of a ceramic rod coated by a conductive metallic film. Note that this type of probe is less delicate compared to a hot-wire probe with the downside being that the larger diameter caused by the ceramic substrate leads to a slower response for extremely high frequency turbulence. Since the wind tunnel in use for this experiment is not capable of producing such high frequency turbulence, this lab utilizes a hot-film probe rather than a hot-wire probe although the terms are used interchangeably throughout this report due to the similar properties of both probes and identical mechanism of measurement performed by both probes. The probe was controlled by a DANTEC 56C Constant Temperature Anemometer (CTA) unit and mounted on a traverse mechanism operated by the Open-Jet Wind Tunnel Operation Control MATLAB code which allowed for the probe to be precisely moved about the cylinder wake. For the purposes of this experiment in identifying critical points in said wake, the probe was only moved vertically in the z-axis through inputs set in the MATLAB wind tunnel operation code.

C. Calibration Technique

The calibration constants A and B required by the King's Law formula shown in Eq. 1 were found using a custom MATLAB script shown in Fig. 4. This script utilizes experimental data that was collected prior to experimentation which contained both the dynamic pressure in inches of water from a pitot-static tube and corresponding mean voltage from the CTA system at various freestream velocities. The script converts the dynamic pressure to Pascals and subsequently calculates the atmospheric density of the lab utilizing the ideal gas law given by equation

$$\rho = \frac{p}{RT} \tag{4}$$

where ρ is the atmospheric density, p is the ambient pressure, R is the universal gas constant, and T is the ambient temperature. The values for the ambient pressure and temperature were gathered during the experiment as 94790 Pa and 294.15 K respectively through the output of the Open-Jet Wind Tunnel Operation Control MATLAB code's GUI. The script subsequently calculates the air velocity using the Bernoulli equation

$$u = \sqrt{2\Delta p/\rho} \tag{5}$$

where Δp is the unit-converted pressure values and ρ is the atmospheric density calculated from Eq. 4. This allowed for the use of a first-order linear polynomial fit to be made on the linearized comparison between E^2 and u^n for $n = 0.45$. The output of this function provided the slope of the best-fit line which is equal to constant B while the y-intercept of said function is equal to constant A allowing for the calibration values to be identified. The script also calculated the required dynamic pressures needed to achieve the target Reynolds numbers for the experiment of 2.0×10^5 and 2.5×10^5 Pa.

D. Experimental Technique

Following calibration, the experiment performed two traversals of the wake for a laminar separation case study and a turbulent separation case study through the use of fan RPMs of 500 and 1000 respectively in order to meet the dynamic pressures found to be required from the calibration step. For the laminar case, the cylinder was rotated such that the trip strip was located such that it faced the jet catcher while the turbulent case had the cylinder rotated such that the trip strip was at a 45-degree angle to the oncoming flow in order to maximize the capability of the strip in producing turbulent flow. In both cases, the hot-film probe traversed along solely the z-axis (i.e. vertically) over a range of ± 7 inches with respect to the cylinder centerline. At discrete 1-inch intervals along this range, the LabVIEW data acquisition system recorded the mean and RMS voltages over a 10-second sampling period which corresponded to 10,000 samples sampled. The voltages were subsequently converted to mean velocity and RMS velocity fluctuations via the use of the calibration constants for the King's Law equations determined in the calibration phase. After traversal, unsteady time history data was collected for 1000 samples at three critical locations. These three critical locations corresponded to the freestream flow, flow at the center of the wake, and flow at the shear layer which were identified from the traversal data by identifying the edge of the traverse (± 7 inches from cylinder centerline), the location of minimum mean velocity (-1 inches from cylinder centerline), and location of maximum RMS fluctuation (± 3 inches from cylinder centerline) respectively.

IV. Results and Discussion

A. Hot-Film Calibration and Uncertainty

The King's Law coefficients found through the calibration procedure described prior were A = 2.520080 V^2 and B = 2.526938 $V^2/(m/s)^{0.45}$. The linearized relationship between $E^2/u^{0.45}$ is shown in blue in Fig. 5 alongside a trendline in red which demonstrates the accuracy of the calibration values to fit the experimental data collected prior to experimentation as described in calibration technique. Furthermore, Fig. 6 depicts the relationship between measured voltage E and predicted velocity u as a non-linear relationship indicating that the sensitivity of the probe decreases as the speed of the flow increases. This figure includes uncertainty bounds which confirm the calibration technique further as all experimental points are within the bounds if not directly on the predicted curve. The larger uncertainty bars at lower velocities are a direct result of the fixed ± 20 Pa uncertainty of the manometer which becomes a larger percentage of the measured dynamic pressure at lower velocities. The data from the calibration step used to generate Fig. 5 and Fig. 6 is found in Table 1 shown below.

Table 1. Hot-film anemometer calibration data and calculated values for King's Law fit.

Δp (Pa)	u (m/s)	δu (m/s)	E (V)	E^2 (V^2)
2.3320	2.0381	8.7397	2.4415	5.9607
11.3253	4.4914	3.9658	2.7366	7.4891
24.8551	6.6538	2.6770	2.9196	8.5241
46.4713	9.0981	1.9578	3.0590	9.3574
71.9528	11.3210	1.5734	3.1738	10.0732
106.3887	13.7660	1.2939	3.2729	10.7116
144.2562	16.0297	1.1112	3.3574	11.2724

185.6343	18.1840	0.9796	3.4400	11.8336
236.5190	20.5254	0.8678	3.5142	12.3496
286.0623	22.5730	0.7891	3.5820	12.8308

The measurements for these values were calculated using the procedure described in calibration techniques and plotted in the aforementioned ways for Fig. 5 and Fig. 6 using the code shown in Fig. 4.

B. Wake Velocity and Turbulence Profiles

The normalized mean velocity profile for the laminar and turbulent boundary layer separation cases are shown in Fig. 7 as orange and blue curves respectively. The vertical axis represents the nondimensionalized position Y/D where Y is the vertical distance from the centerline (i.e. the position along the traversed range of ± 7 inches along the vertical z-axis) and D is the cylinder diameter of 5.5 inches. The horizontal axis represents the nondimensionalized mean velocity $\bar{u}/u_e$ where $\bar{u}$ is the mean velocity as given by Eq. 2 and u_e is the freestream velocity outside of the wake which, as mentioned in the experimental technique section, is the velocity recorded by the hot-film probe at ± 7 inches along the vertical z-axis. A value for $\bar{u}/u_e < 1$ implies that the flow has not recovered to the undisturbed freestream velocity following a disturbance which is the defining physical characteristic of a wake. From this property, it can be garnered that the curve for the laminar case shown in orange on Fig. 7 exhibits a much larger deficit in the velocity at the wake as the velocity at the centerline drops to approximately 28% of the freestream value. In contrast, the curve for the turbulent case shown in blue on Fig. 7 exhibits a less severe deficit as the minimum velocity at the centerline is approximately 35% of the freestream value. This causes the overall curve for the turbulent case to be "shifted" to the right relative to the laminar curve. This rightward shift is a result of the difference between the behavior of the boundary layer on the cylinder surface prior to flow separation as the laminar boundary layer is defined by a smooth flow of relatively low momentum fluid which is more likely to separate early and cause a larger, wider wake compared to the turbulent boundary layer with higher levels of momentum leading to a better capability in resisting separation behind the cylinder and correspondingly a narrower wake with a smaller deficit in the mean velocity. This difference in the separation of flow past a cylinder for laminar versus turbulent boundary layer separation can be seen in Fig. 8 where the sub-critical Reynolds number flow corresponds to a more laminar flow and thus has a earlier separation and larger wake compared to the super-critical Reynolds number flow which corresponds to a more turbulent flow and thus has a later separation and much narrower turbulent wake.

C. Unsteady Time-History Velocity Measurements

The time-history of the instantaneous velocity at the three critical locations corresponding to the freestream flow, flow at the center of the wake, and flow at the shear layer as described in experimental techniques is shown in Fig. 9, 10, and 11 respectively. As aforementioned, these correspond to a probe location of ± 7, ± 3, and -1 inches for the respective critical locations along the vertical z-axis. In each figure, the horizontal axis represents time while the vertical axis represents the velocity in meters per second.

Notable qualitative differences can be gleaned from comparison between the figures. Specifically, Fig. 9 depicts a higher average velocity of 11.333 m/s compared to the average velocities of 3.1814 and 2.7427 m/s in Fig. 10 and 11 respectively. Furthermore, the signal is far smoother with relatively small-amplitude fluctuations that are relatively minor compared to the average velocity. Thus, as expected for the region of freestream flow, the turbulence intensity is low and the flow far from the cylinder is generally uniform and stable. Conversely, the wake center and shear layer have far more turbulent flow with the shear layer having the greatest intensity of turbulence and lowest average velocity signaling the greatest deficit in comparison with the freestream flow velocity. These properties are expected as the Kármán vortex street created in the wake of a cylinder sheds large-scale vortices which pass through the wake 's centerline and creates large swings in measured velocity while the shear layer contains the largest fluctuations in velocity as it defines the interface between the relatively low velocity wake and the relatively high velocity freestream. The large gradient between the interface creates a mechanism for turbulence intensification as eddies of varying sizes are created. This visualization thus confirms why the RMS velocity profile contains distinct peaks at the edges rather than the centerline of the wake since the edges of the wake define the location of the shear layer and RMS allows for a measure of the turbulence intensity.

V. Conclusion

This investigation successfully performed hot-film anemometry to characterize the fluid flow in the wake of a cylinder and highlighted the differences between laminar and turbulent flows' boundary layer separation. Te experimental procedure required the calibration of the hot-film probe via the derivation of constants A and B from the King's Law response equation given by Eq. 1. The procedure further involved the systematic traversal of the hot-film probe across the cylinder wake to measure the mean velocity curves for both laminar and turbulent cases and identify critical characterizing locations of the flow to enable subsequent time-history data acquisition for analysis of the unsteady nature of the flow. The results validated fundamental aerodynamic principles and demonstrated the unique capabilities of hot-wire anemometry for research and testing in turbulent flow regimes due to the capacity for hot-wire and hot-film probes to acquire data at high-sampling rates.

The most significant result of this investigation is the profound impact the boundary layer state has on the downstream wake structure as the wake formed from laminar separation is substantially wider and thus contains a larger deficit in velocity, and thus momentum, compared to the wake formed from turbulent separation caused by a induced tripping of the boundary layer. This is a direct result of the differences in momentum of the fluid flow for laminar versus turbulent cases as the lower velocity, and thus lower energy, flow is more susceptible to the pressure gradient on the aft surface of the cylinder, leading to an early separation, wider wake, and greater deficit in velocity compared to the freestream. On the other hand, the turbulent regime contains flow of higher velocity, and thus energy, which leads to a greater momentum and ability to resist the pressure gradient in the rear of the cylinder, leading to later separation and thus narrower wake with a smaller deficit in velocity compared to the freestream. Furthermore, the unsteady time-history data confirmed the relatively calm freestream flow and implied at the existence of both vortex shedding at the wake's center as well as the creation of chaotic eddies at the shear layer alongside a qualitative measure of turbulence intensity implying the shear layer's greater turbulence than the center of the wake.

The implications of these results are profound and form the basis for drag-based design in aerodynamic engineering as the narrower wake and smaller velocity deficit leads to a reduction in pressure drag shown by the equation

$$C_d = -\frac{1}{2}\int_0^{2\pi} C_p(\theta)\cos\theta \, d\theta \tag{6}$$

where C_d is the nondimensionalized drag coefficient, $C_p(\theta)$ is the pressure coefficient as a function of the angular position theta about the cylinder measured from fore to aft, and $\cos\theta$ projects the surface pressure in the direction of the freestream velocity. This equation directly links the distribution of the surface pressure about the cylinder to the net drag force experienced by the cylinder and demonstrates the effect the location of separation has on drag. Specifically, for an early flow separation as seen in laminar regimes, a lower pressure region is created for an extended region over the rear of the cylinder which leads to a lower $C_p(\theta)$ over a larger region than the turbulent case particularly in a region where $\cos\theta$ is also negative. Therefore, the integral accumulates a larger negative contribution and thus, when multiplies by the $-\frac{1}{2}$, the value of C_d and thus the value of net drag becomes more positive. The turbulent regime allows for the oppositive to happen as the region of lower pressure is moved further aft and thus $C_p(\theta)$ recovers such that it is less negative over the rear surface resulting in a smaller negative value for the integral and thus a smaller net drag.

Thus Eq. 6 combines with the experimentally identified wake properties of laminar and turbulent regimes to justify the theoretical aerodynamic principle of turbulent separation resulting in higher surface pressure and lower overall pressure drag, even through induced means of separation. This connection forms a cornerstone of aerodynamic design where mechanisms of inducing turbulent separation can significantly reduce pressure drag by reshaping the wake structure to a more aerodynamically favorable form.

In summary, the following conclusions can be garnered from this investigation:

1. The hot-film anemometer calibration allowed experimental determination of King's Law coefficients $A = 2.520080\ V^2$ and $B = 2.526938\ V^2/(m/s)^{0.45}$ which confirms a decrease in probe sensitivity at higher velocities. Further, through use of the calibration coefficients plotted against data collected prior to experimentation, the calibration coefficients were further justified in their veracity due to a close fit as shown in Fig. 5.
2. Inducing turbulent boundary layer separation through physical mechanisms such as a trip strip leads to a narrower wake and smaller difference between wake and freestream velocity compared to natural separation from laminar flow.

3. The highest levels of turbulence intensity, as measured by the fluctuations in RMS velocity, were found at the edge of the wake, which is defined as the shear layer, rather than the centerline of the wake. This was confirmed both numerically by the wake traversal curve as well as qualitatively by the time-history curve.

From the results of this investigation, the experimental methodology was proven to be effective as the calibration technique allowed for an accurate basis for subsequent measurements and the use of a trip strip was successful in simulating the effects of supercritical Reynolds number flow. However, some sources of uncertainty are of note, particularly regarding the manometer's fixed uncertainty of ± 20 Pa uncertainty which is more significant at low dynamic pressures used for lower velocity calibration points. Furthermore, due to constraints the calculation of the King's Law exponent was set as $n = 0.45$ without determining the constant experimentally. However, this value was provided as a fairly standard value for hot-wire probes. Despite these limitations, the experimental results qualitatively agree with established aerodynamic theory allowing a certain confidence to be made of the conclusions drawn regarding the differences between laminar and turbulent flows' boundary layer separation.

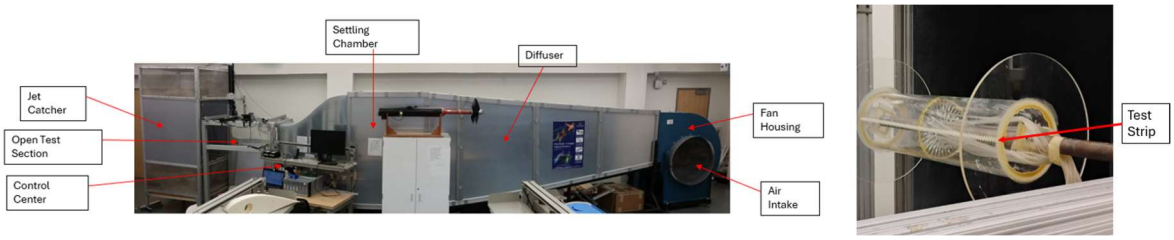

Fig. 1. Wind Tunnel Annotated. Adapted from Borgoltz (2024).

Fig. 2. DANTEC 56C Constant Temperature Anemometer (CTA) System.

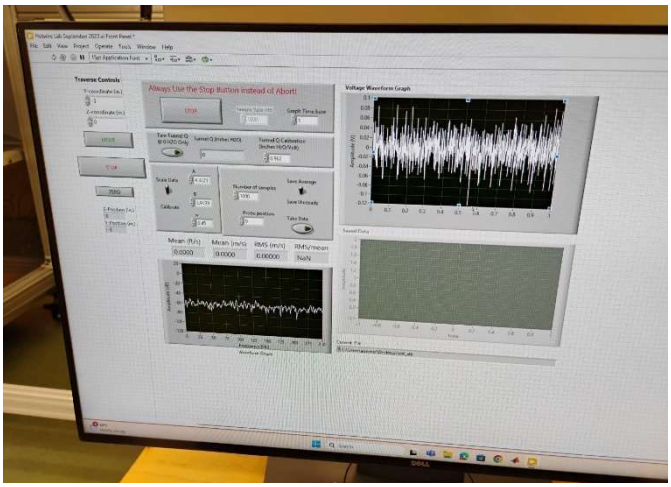

Fig. 3. LabVIEW Data Acquisition Software.

```
deltap = 249.089 * [0.15, 0.21, 0.44, 0.74, 1.01, 1.47, 1.89, 2.42]'; % in H2O to Pa
E = [2.93, 3.05, 3.22, 3.35, 3.46, 3.56, 3.65, 3.72]';
p_atm = 99200; % pa
T_atm = 296.55; %K
R = 287;
n = 0.45;
uncertainty = 20;
rho = p_atm / (R*T_atm);
fprintf("Rho: %f kg/m^3 \n", rho);
u = sqrt(2*deltap / rho);
deltau = (10*u) ./ (deltap);
x_fit = u.^n;
y_fit = E.^2;
coeffs = polyfit(x_fit, y_fit, 1);
B = coeffs(1);
A = coeffs(2);
fprintf('  A: %f [V^2]\n', A);
fprintf('  B: %f [V^2 / (m/s)^%f]\n\n', B, n);
figure('Name', 'Plot 1');
plot(x_fit, y_fit);
hold on;
plot(x_fit, A + B*x_fit);
grid on;
xlabel('u^0.4 [(m/s)^.45]');
ylabel('E^2 [V^2]');
title('King''s Law Calibration: E^2 vs u^n');
hold off;
upred = ((E.^2 - A) / B).^(1/n);
figure('Name', 'Plot 2');
errorbar(E, u, deltau);
hold on;
E_smooth = linspace(min(E), max(E), 100);
u_smooth = ((E_smooth.^2 - A) / B).^(1/n);
plot(E_smooth, u_smooth);
grid on;
xlabel('E [V]');
ylabel('u [m/s]');
title('King''s Law Prediction vs Data');
hold off;
D = 5.5 * 0.0254; % m
Re = [2e5, 2.5e5];
mu = 1.81e-5;
for i = 1:length(Re)
    u_req = (Re(i) * mu) / (rho * D);
    dp = 0.5 * rho * u_req^2;
    dpinH2O = dp / 249.089;

    fprintf('Re = %e\n', Re(i));
    fprintf('  u = %f m/s\n', u_req);
    fprintf('  deltap = %f Pa\n', dp);
    fprintf('  deltap = %f inH2O\n\n', dpinH2O);
end
```

Fig. 4. Calibration MATLAB Script (with Temporary p_atm and T_atm Values).

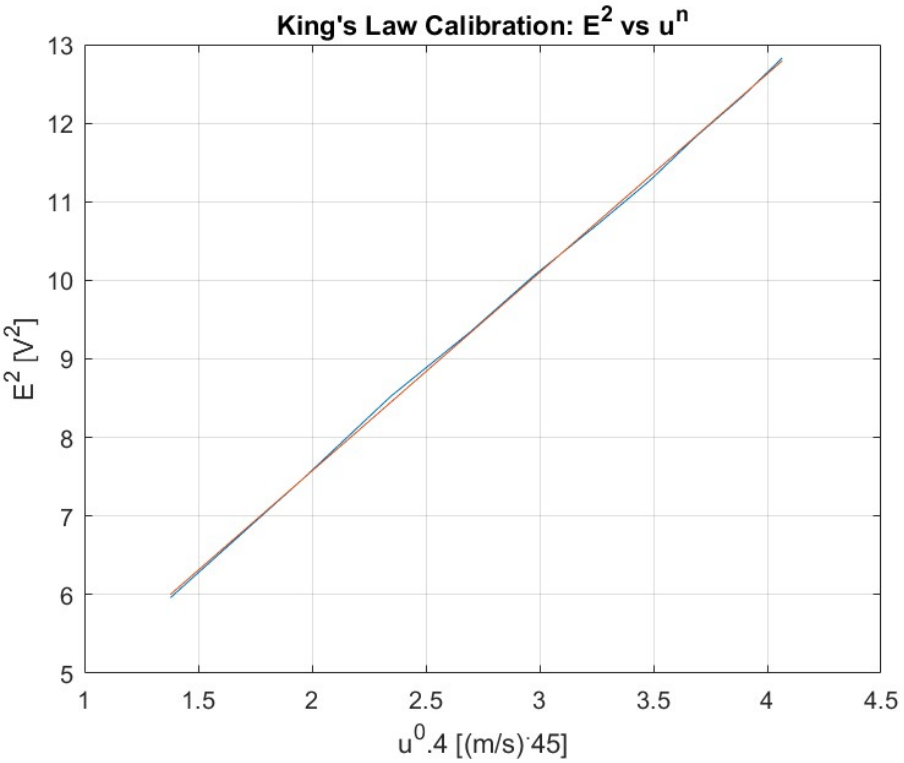

Fig. 5. Linearized Relationship between $E^2/u^{0.45}$

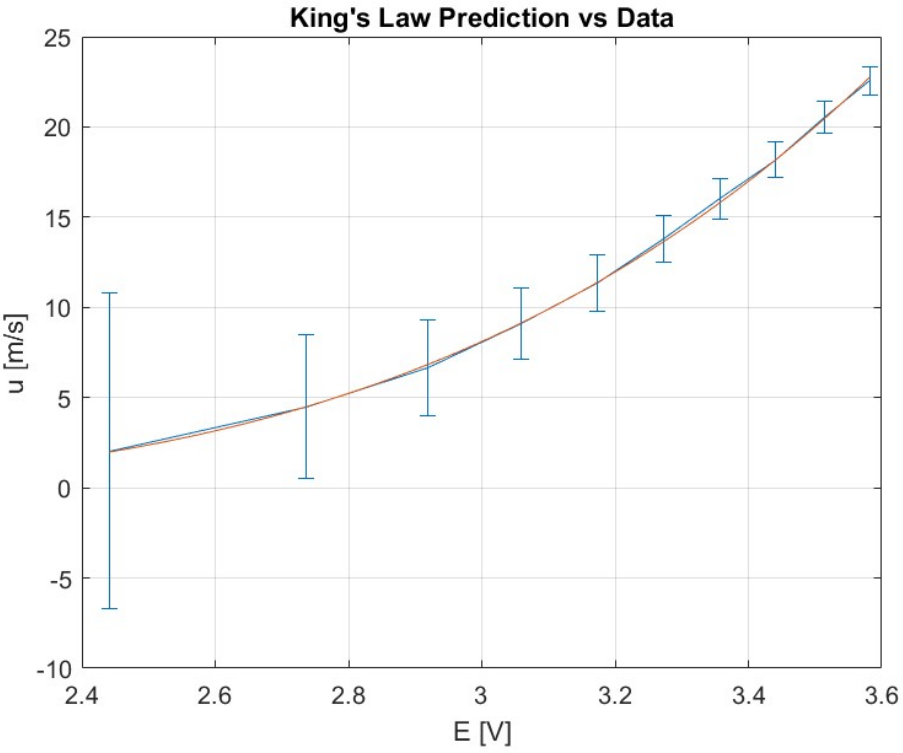

Fig. 6. Relationship between E/u.

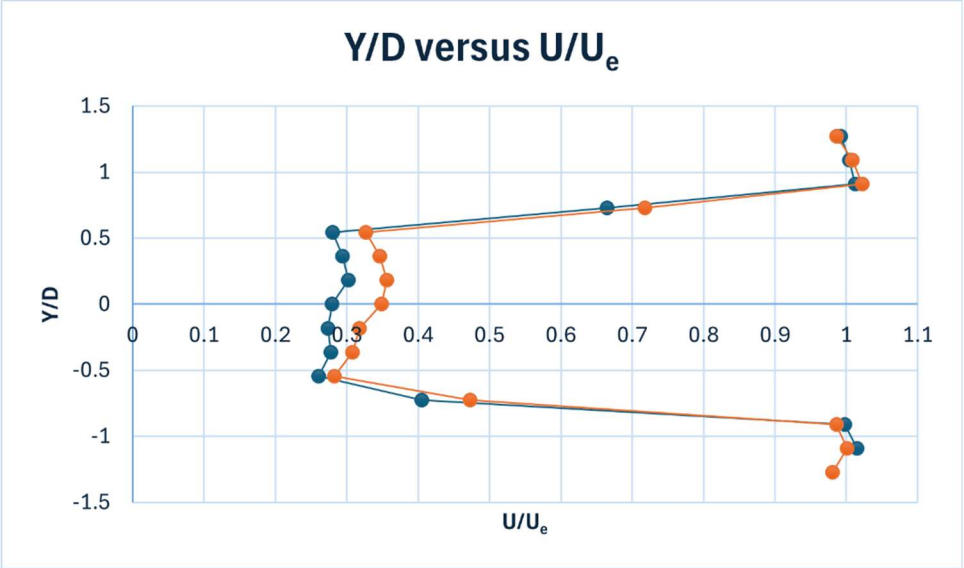

Fig. 7. Schematic of the excitation system. From Hallauer and Devenport (2006).

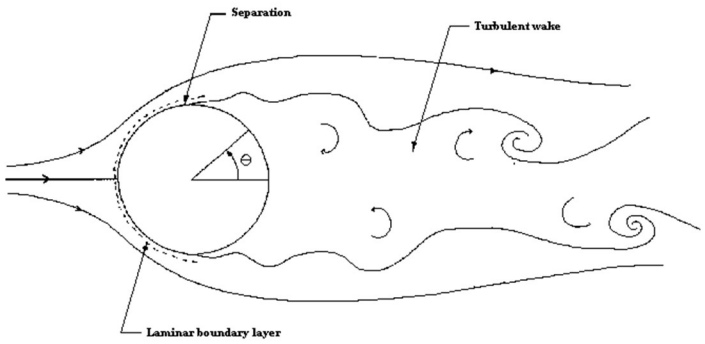

(a) Sub-critical Reynolds number

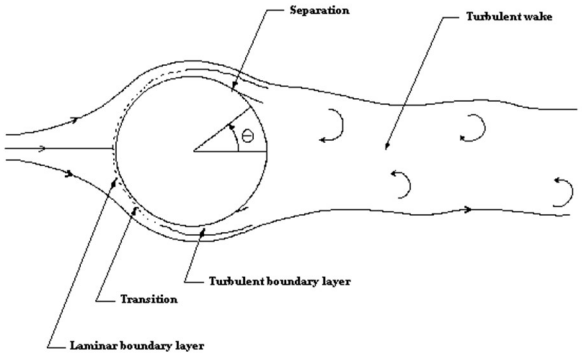

(b) Super-critical Reynolds number

Fig. 8. Flow Past a Cylinder for Sub-critical versus Super-critical Reynolds numbers.

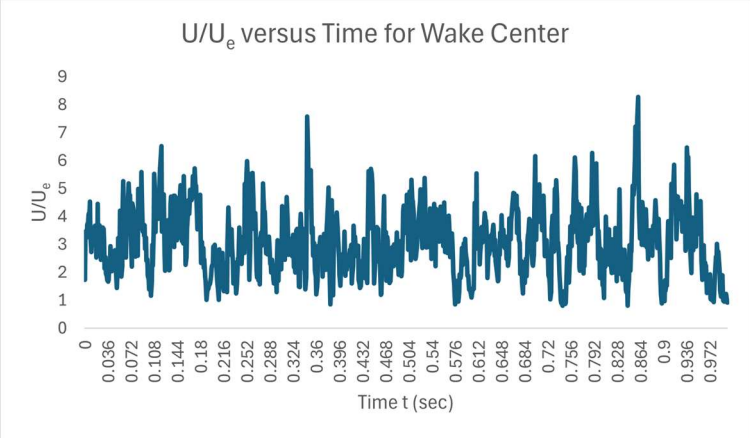

Fig. 9. Time-history Data for Probe at -1 Inches from Cylinder Centerline (Wake Center).

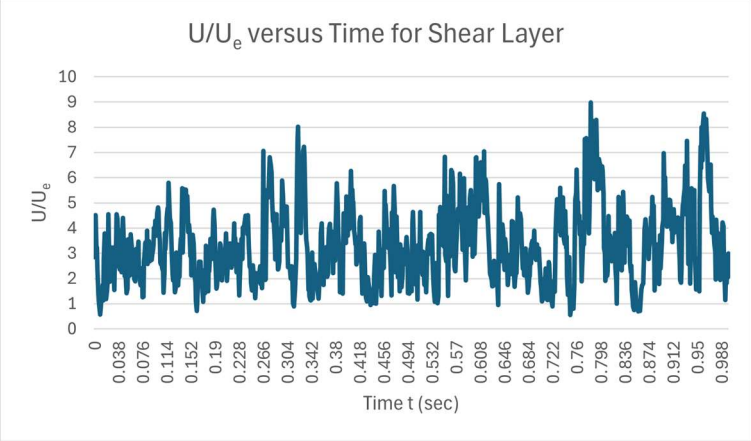

Fig. 10. Time-history Data for Probe at +3 Inches from Cylinder Centerline (Shear Layer).

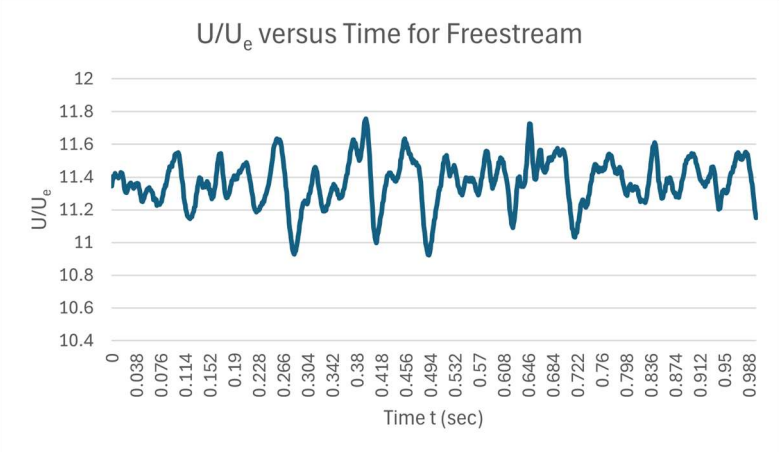

Fig. 11. Time-history Data for Probe at +7 Inches from Cylinder Centerline (Freestream).

REFERENCES

A. Borgoltz, W. Devenport, and N. Intaratep, "AOE3054 — Experiment 3: Flow Past a Circular Cylinder," Virginia Polytechnic Institute and State University, Apr. 1, 2025. [Online]. Available: https://www.aoe.vt.edu/instruction/aoe3054/expt3.html [Accessed: Sep. 26, 2025].

D. Neu, "Hot-Wire Anemometry Experiment," AOE 4154 Hot Wire Lab, Virginia Polytechnic Institute and State University, archived. [PDF]. Available: https://archive.aoe.vt.edu/simpson/aoe4154/hotwirelab.pdf [Accessed: Sep. 28, 2025].

Appendix A

A. Uncertainty Analysis

Uncertainties in derived quantities are calculated using the root-sum-square (RSS) method and are reported for 20:1 odds such that a 95% confidence interval is had such that true values lie within the range defined by the . This means there is a 95% probability that the true value of the measurement lies within the range defined by the value $\pm$ its uncertainty.

To obtain the uncertainty in for variables dependent on several measured variables, the uncertainties are combined using the equation

$$\delta(R) = \sqrt{\left(\frac{\partial R}{\partial a}\delta(a)\right)^2 + \left(\frac{\partial R}{\partial b}\delta(b)\right)^2 + \left(\frac{\partial R}{\partial c}\delta(c)\right)^2 + \cdots} \tag{7}$$

where the variables a,b,c… are the variables measured that R depends on. The most notable uncertainty in this experiment is the uncertainty in the calibration velocities The most critical uncertainty in this experiment is the uncertainty in the calibration velocities δu since this uncertainty propagates through the entire investigation. The velocity u is calculated from the measurement for dynamic pressure Δp made by the manometer which has a given uncertainty of $\pm$ 20 Pa. This uncertainty propagates through the equation

$$u = \sqrt{\frac{2\Delta p}{\rho}} \tag{8}$$

where ρ is the atmospheric density of the lab as measured by the pitot-static probe and output onto the GUI of the Open-Jet Wind Tunnel Operation Control MATLAB code. By applying Eq. 7 with $a = \Delta p$ and $b, c, \ldots = 0$ onto Eq. 8 uncertainty in velocity can be derived as

$$\delta u = \left|\frac{\partial u}{\partial(\Delta p)}\right| \delta(\Delta p) = \frac{1}{\rho u}\delta(\Delta p) \tag{9}$$

Applying Eq. 9 onto each calibration point provides the uncertainties in velocity per calibration sample, which was performed as part of the investigation as shown in the script in Fig. 4 and the resulting plot in Fig. 6. Furthermore, these tabulations are provided in Table 2 found below.

Table 2. Uncertainty Propagation from Measured Dynamic Pressure.

Δp (Pa)	u (m/s)	$\delta(\Delta p)$ (Pa)	δu (m/s)	δu/u (%)
2.3320	2.0381	$\pm$20	8.7397	428.8161
11.3253	4.4914	$\pm$20	3.9658	88.2976
24.8551	6.6538	$\pm$20	2.6770	40.2326
46.4713	9.0981	$\pm$20	1.9578	21.5188
71.9528	11.3210	$\pm$20	1.5734	13.8981
106.3887	13.7660	$\pm$20	1.2939	9.3992
144.2562	16.0297	$\pm$20	1.1112	6.9321

Note that the large relative uncertainty seen for lower values of Δp are a result of the fixed nature of the manometer uncertainty which results in the progressively smaller error bars seen in Fig. 6 as well as smaller uncertainties δu for larger velocities. As mentioned in the conclusion, the uncertainty is not of enough significance to invalidate the conclusions drawn from the investigation, especially as conclusions match established aerodynamic theory.